International Journal of Heat and Mass Transfer 52 (2009) 4894–4900

Contents lists available at ScienceDirect

International Journal of Heat and Mass Transfer

journal homepage: www.elsevier.com/locate/ijhmt

A three-dimensional numerical simulation of impinging jet arrays on a moving plate

L.B.Y. Aldabbagh [a,*], A.A. Mohamad [b]

[a] Mechanical Engineering Dept., Eastern Mediterranean University, Magosa, Mersin 10, Turkey
[b] Dept. of Mechanical and Manufacturing Engineering, The University of Calgary, Calgary, AB, T2N 1N4, Canada

ARTICLE INFO

Article history:
Received 30 January 2009
Received in revised form 14 May 2009
Accepted 14 May 2009
Available online 9 July 2009

Keywords:
Moving surface
Jet arrays
Impinging jet

ABSTRACT

The structure of the flow field and its effect on the heat transfer characteristics of a jet array system impinging on a moving heated plate are investigated numerically for Reynolds numbers between 100 and 400 and for steady state conditions. An array consisting of 24 square jets (3 rows × 8 columns) impinging on a moving heated flat surface is considered as a representative pattern.

The simulations have been carried out for jet-to-jet spacing in the range 2*D*–5*D* and for nozzle exit to plate distance of 0.25*D*, where *D* is the jet width. The velocity ratios of the moving heated plat to the jet velocity ($R_m = u_p/u_j$) used are in the range 0.25–1.0. The obtained results were compared with published data for the case of fixed heated plate ($R_m = 0.0$). The results show that the streamwise profile of the Nusselt number exhibit strong periodic oscillations, spatially. The amplitude of the periodic oscillations of the Nusselt number is attenuated as one proceeds in the downstream direction. For such small nozzle-to-plate spacing used, the results show that the ratio R_m has no effect on the oscillations of Nusselt number.

1. Introduction

Impinging jets are extensively used to provide rapid cooling or drying in a large number of applications. Among these applications are the tempering of glass, drying of paper and textiles, cooling of metal sheets, micro-electronic components and turbine blades. However, the high heat transfers rates which occur in the impingement regions of the jets decays rapidly away from the stagnation zones. In submerged jet arrays the exhaust from the upstream jets imposes a crossflow on the downstream jets. The crossflow effect and the interaction between the jets cause variations in the heat transfer performance of individual jets in an array which can affect the quality of the product in material processing. Jet interaction produces a rather complex flow field in the array. The inclusion of impingement surface motion adds another level of complexity in the analysis due to the present of strong shear regions. Therefore a three-dimensional modeling is necessary in order to get a basic understanding of the essential dynamics of the flow field.

There is a large number of experimental works related to impingement heat transfer in jet arrays. Gardon and Akfirat [1] carried out an early work to measure the heat transfer coefficients of two-dimensional slot jets impinging perpendicular to an isothermal flat plate. The influence of crossflow caused by the spent air on heat transfer in jet array systems has been investigated by Kercher and Tabakoff [2], Metzger et al. [3], Florschuetz et al. [4] and Obot and Trabold [5]. These studies show that crossflow and adjacent jet interactions decrease the magnitude of heat transfer coefficient of individual jets in an array. Heat transfer characteristics of liquid jet arrays impinging normal to a heated isoflux plate has been studied experimentally by Garrett and Webb [6] for different jet-to-jet spacing and height of nozzles. The data revealed strong spatial oscillations in the local Nusselt number along streamwise direction. Moreover, crossflow has the effect of transforming the concentric isotherms around the stagnation point into elliptical shape. All of the mentioned works considered jet array impingement on a stationary surface.

Among very few experimental studies involving jets impinging on a moving flat surface is the work of Subba Raju and Schlunder [7], concerning a moving flat surface impinged by a turbulent slot air jet. The experiment was performed for different nozzle-to-plate spacing, several Reynolds numbers and the surface velocity between 0.15 m/s and 5.5 m/s were considered. Van Heiningen et al. [8] conducted an experimental study of a turbulent slot air jet impinging on a large rotating drum. The tangential velocity of the moving surface was less than 2% of the jet velocity. Comparing their results with publish data for a turbulent slot jet impinging on a stationary surface, they concluded that, for low surface-to-jet velocity ratios, the effect of the wall motion seemed to be negligible on the local heat transfer. The flow field of a confined turbulent slot air jet impinging normally on a flat surface has been investigated experimentally by Senter and Solliec [9]. The experiments were conducted for a nozzle-to-plate spacing of eight slot nozzle widths, at three Reynolds number (5300, 8000, and 10,600) and for surface-to-jet velocity ratios (0, 0.25, 0.5, and 1.0). They concluded that, a slight modification of the flow field is observed for

* Corresponding author. Fax: +90 392 3653715.
E-mail address: loay.aldabah@emu.edu.tr (L.B.Y. Aldabbagh).

0017-9310/$ - see front matter © 2009 Elsevier Ltd. All rights reserved.
doi:10.1016/j.ijheatmasstransfer.2009.05.020

Nomenclature

A_x, A_y, A_z	aspect ratios in x, y and z-direction, L_x/D, L_y/D, L_z/D
D	jet width (m)
h	heat transfer coefficient (W/m^2 K)
L_x, L_y, L_z	length of heated surface in x, y and z-directions, respectively (m)
k	thermal conductivity (W/m K)
Nu	local Nusselt number (hD/k)
p	pressure (N/m^2)
P	non-dimensional pressure ($p/\rho u_j^2$)
Pr	Prandtl number (ν/α)
q''_w	local convective heat flux at the impingement plate
Re	jet Reynolds number (u_jD/ν)
R_m	velocity ratios of the moving heated plat to the jet velocity (u_p/u_j)
t	temperature (K)
T	non-dimensional temperature, $(t - t_j)/(t_w - t_j)$
u_j	jet exit velocity (m/s)
u_p	plate velocity (m/s)
u, v, w	Cartesian velocities
U	non-dimensional Cartesian velocity, in x-direction (u/u_j)
V	non-dimensional Cartesian velocity, in y-direction (v/u_j)
W	non-dimensional Cartesian velocity, in z-direction (w/u_j)
x, y, z	Cartesian coordinates
X_n, Y_n	jet–jet spacing in x and y-directions, respectively
X, Y, Z	non-dimensional Cartesian coordinates, x/D, y/D, z/D, respectively

Greek symbols

α	thermal diffusivity (m^2/s)
ν	kinematic viscosity (m^2/s)
ρ	density (kg/m^3)
ϕ	U, V, W, P, or T field

Subscripts

j	jet exit
w	wall

a surface-to-jet velocity ratio of 0.25 whereas at higher ratios, the flow field is significantly affected.

Several numerical studies have been present of a slot jet impinging on a moving flat plate. Yang and Hao [10] presents result for three turbulent impingement slot jets with and without moving surface. They found that the heat transfer characteristic is not significant in the range of $0.05 \leqslant R_m \leqslant 0.25$. Chen et al. [11] and Zumbrunnen [12] have shown that the movement of the impingement surface strongly influences the flow field and heat transfer characteristics. However, they had considered a numerical model for convection heat transfer within an array of submerged planar jets impinging on a moving surface with uniform heat flax and constrained their study mainly in the laminar regime. Zumbrunnen et al. [13] published analytical model for a single laminar impinging slot jet on an isothermal and isoflux moving plate. They showed that the heat transfer is more effective due to the slowing down of the boundary layer development away from the jet by the plate moving. Chattopadhayay et al. [14] numerical investigated turbulent heat transfer from a moving plate due to an array of impinging slot jets for jet exit Reynolds number ranging between 500 and 3000. They concluded that the span averaged Nusselt number distribution over the plate becomes more uniform while the total heat transfer reduces with increasing plate speed. Similar conclusions were reported by Chattopadhayay and Saha [15] by investigated the laminar heat transfer from a moving plate due to an array of impinging slot jets within a jet exit Reynolds number range of 100–200. Later, Chattopadhayay [16] numerically studied the effect of surface motion on transport processes due to circular impinging jets in both laminar and turbulent regime. One circular jet in a symmetry domain with crossflow was used in the simulation. He presented results for only one normalized jet-to-plate spacing of 2 for jet exit Reynolds number between 100 and 2500 with normalized plate velocities of 0–1. The normalized domain length of his computation was 10. The numerical prediction indicated that, the surface velocity influences strongly the flow structure over the impinging surface, leading into reduction in heat transfer.

The studies of [17–21] focus on a turbulent single jet impinging on a moving surface for different jet exit Reynolds number, jet-to-plate spacing, and with normalized plate velocities of 0–2. They reported that the average Nusselt number increases considerably with the jet exit Reynolds number as well as with the plate velocity.

In practice, the jets are generally turbulent. However, turbulence models lack generality due to the wide range of scales they employ. On the other hand the three-dimensional flow structure resulting from laminar jet arrays impinging on a moving surface is far from being fully understood. In this study we use a three-dimensional laminar flow model in order to obtain a detailed flow structure for such a complex configuration. A section of an array consisting of 24 square jets (3 rows × 8 columns) impinging on a moving heated flat surface is considered as a representative pattern (Fig. 1). The first column at the left side represents the central portion of the array. The structure of the flow field and its effect on the heat transfer characteristics are investigated numerically for Reynolds numbers between 100 and 400 and for three difference plate velocities ratios (0.25, 0.5, and 1.0).

2. Computational scheme

The flow and heat transfer is described by the three-dimensional continuity, Navier–Stokes and energy equations in Cartesian coordinates. The velocity and lengths are non-dimensionalized by jet exit velocity and jet width, respectively. The buoyancy effect has been neglected to separate the effects of various parameters. Thus the results are valid for Richardson number less than unity, where buoyancy effects are negligible. The governing equations in non-dimensional form are

$$\frac{\partial U}{\partial X} + \frac{\partial V}{\partial Y} + \frac{\partial W}{\partial Z} = 0 \tag{1}$$

$$U\frac{\partial U}{\partial X} + V\frac{\partial U}{\partial Y} + W\frac{\partial U}{\partial Z} = -\frac{\partial P}{\partial X} + \frac{1}{Re}\nabla^2 U \tag{2}$$

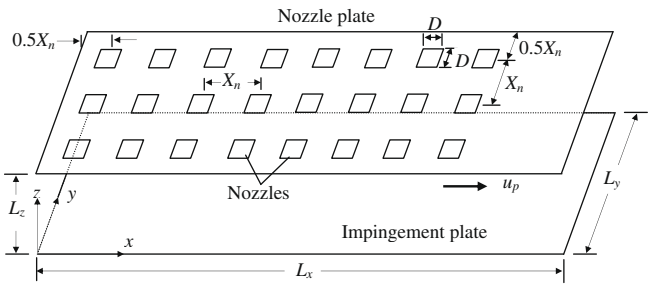

Fig. 1. Schematic diagram of the physical model and the coordinate system.

$$U\frac{\partial V}{\partial X}+V\frac{\partial V}{\partial Y}+W\frac{\partial V}{\partial Z}=-\frac{\partial P}{\partial Y}+\frac{1}{Re}\nabla^2 V \quad (3)$$

$$U\frac{\partial W}{\partial X}+V\frac{\partial W}{\partial Y}+W\frac{\partial W}{\partial Z}=-\frac{\partial P}{\partial Z}+\frac{1}{Re}\nabla^2 W \quad (4)$$

$$U\frac{\partial T}{\partial X}+V\frac{\partial T}{\partial Y}+W\frac{\partial T}{\partial Z}=\frac{1}{Re\,Pr}\nabla^2 T \quad (5)$$

where T is the non-dimensional temperature, $(t-t_j)/(t_w-t_j)$.

2.1. Boundary conditions for velocities

Fig. 1 shows the schematics of the array of square jets impinging on a moving plate. The middle row of jets, which is located at $Y = 0.5L_y$, is surrounding by two rows. The additional two rows were added to study the affect of the surrounding jets on the mid row jets. The surface plate is moving in one direction from left to right. As a result, symmetry conditions are used at $Y = 0$ and $Y = L_y$. The outlet boundary of the flow is located far enough downstream for conditions to be substantially developed. No-slip boundary condition is used for the top solid wall except that the velocity is specified at the exit of the jets, where it is assumed to be uniform and is set to be equal to unity. The bottom solid plate is assumed to move with velocity ratio $R_m = u_p/u_j$. Accordingly, the following non-dimensional boundary conditions are imposed:

$$U=\frac{\partial V}{\partial X}=\frac{\partial W}{\partial X}=0 \quad \text{at } X=0$$

$$\frac{\partial U}{\partial X}=V=W=0 \quad \text{at } X=A_x$$

$$V=\frac{\partial U}{\partial Y}=\frac{\partial W}{\partial Y}=0 \quad \text{at } Y=0,\ Y=A_y$$

$$U=R_m,\ V=W=0 \quad \text{at } Z=0$$

$$U=V=W=0 \quad \text{at } Z=A_z \text{ except at nozzle exit,}$$

$$U=V=0,\ W=-1 \quad \text{at nozzle exit.}$$

2.2. Boundary conditions for temperature

If the fluid exits the domain (at right) the first derivative of temperature is set to zero and if the fluid flows from surroundings into the domain then the fluid temperature is set to the surrounding temperature. Symmetry conditions are imposed at the left, front, and rear sides. Adiabatic boundary conditions are used on the top wall, except at the nozzles exit cross section where it was set to be equal to that of ambient. The bottom plate is set to a higher temperature than the ambient. Accordingly,

At $X=0$	$\frac{\partial T}{\partial X}=0$	
At $X=A_x$	$\frac{\partial T}{\partial X}=0$	for $U>0$
	$T=0$	for $U<0$
At $Y=0,\ Y=A_y$	$\frac{\partial T}{\partial Y}=0$	
At $Z=0$	$T=1$	
At $Z=A_z$	$\frac{\partial T}{\partial Z}=0$	except at nozzle exit
	$T=0$	at nozzle exit.

3. Method of solution

The governing equations are discretized by using the finite volume method in staggered, nonuniform grids. The grids are generated such that denser grid clustering is obtained in the vicinity of the jets in x and y-directions. In the z-direction a sine function distribution is employed, yielding denser grids near the top and near the impingement plate. A grid independence test has been made for $Re = 200$, $R_m = 0$, and $X_n = 5$ in order to determine the effect of the number of grids on the final results. The maximum difference between the results obtained by using $450 \times 156 \times 54$ and $338 \times 116 \times 40$ grids is 2.5% for the local Nusselt number. The corresponding difference between $338 \times 116 \times 40$ and $254 \times 90 \times 30$ grids is 6.7%. Hence, the $338 \times 116 \times 40$ grid system is used in the simulations. The solution domain has $L_x = 47.5D$ and $L_y = 3X_n$ in x and y-directions, respectively. Special treatment of the advective flux is required to accurately capture the velocities in the high gradient regions around the jet. QUICK scheme [22] is used to calculate the convection of a scalar term, ϕ at a control-volume face. However, this scheme is not bounded and cause oscillations in sharp gradient regions. Many remedies have been proposed. A common approach involves using high-resolution flux limiters. These limiters are based on composite flux expressions which insure boundedness in regions of sharp gradients and also provide high resolution in monotonic regions. In this work the ULTRA-SHARP flux limiter [23,24] is used to enforce monotonicity. The flux term is applied using a deferred correction technique to reduce the stencil of the discrete equations. In this technique the flux value estimated by the QUICK scheme is written as the sum of the first-order upwind term plus a correction term, which provides higher accuracy. The first-order upwind term is treated implicitly, while the correction term is treated explicitly and added to the source term. The procedure guaranties that the discrete system of equations is diagonally dominant, which is important for iterative solvers. In addition the seven diagonal structure of the coefficient matrix is preserved, which does not require extra storage. The discretized mass momentum and energy equations are solved in a segregated approach using the standard SIMPLEC [25] algorithm. The momentum equations are solved by using the iterative method SIP of Stone [26], which is extended here to handle three-dimensional problems. The pressure-correction equation yields a symmetric coefficient matrix, which is solved by using the conjugate gradient method [27]. The coefficient matrix resulting from the energy equation is nonsymmetric and is solved by Bi-CGSTAB [28] iterative method. The coefficient matrices are preconditioned by SSOR method [29] in order to speed up convergence rate of the iterative solvers. An under relaxation factor of 0.5 is used for momentum and 0.7 for energy equations in all calculations. Iterations are continued until the second norm of the residuals for all equations are reduced below 10^{-6}, where no significant variations are observed at this residual level. In the absence of experimental data under identical conditions the validation of numerical code was performed against the experimental measurements of Sparrow and Wong [30], who used a developed slot-jet flow impinging on a naphthalene plate. The results are presented in a previous

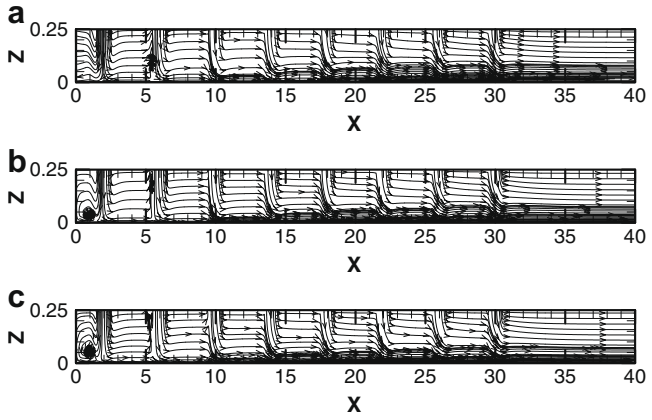

Fig. 2. Projection of flow lines on mid x–z plane for $Re = 200$, $X_n = 4$, and for surface velocity ratio (a) $R_m = 0.0$, (b) $R_m = 0.5$, and (c) $R_m = 1.0$.

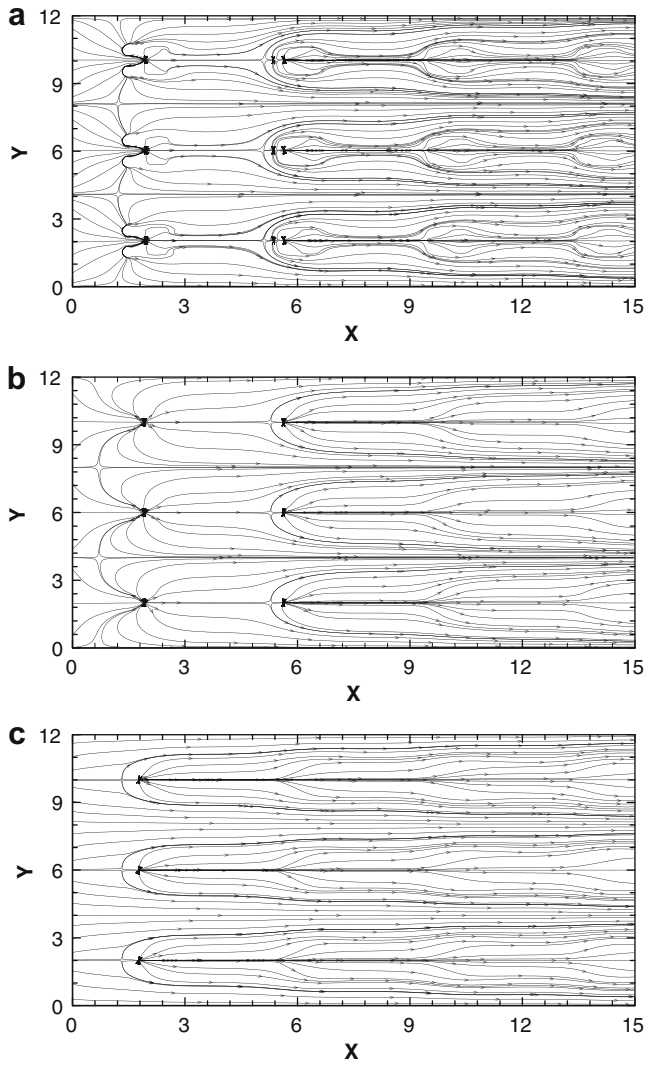

Fig. 3. Projection of flow lines for $Re = 200$, $R_m = 1.0$, and $X_n = 4$ on horizontal cross section at (a) $Z = 0.225$, (b) $Z = 0.125$, and (c) $Z = 0.025$.

publication by Aldabbagh and Sezai [31]. The agreement between the numerical results and the experimental measurements is in general satisfactory.

4. Results and discussions

Air is used as the working fluid, having a Prandtl number of 0.71. The analysis is performed for Reynolds numbers between 100 and 400, and for the surface velocity ratios, $R_m = u_p/u_j$, between 0.25 and 1.0. The aspect ratios, $A_z = L_z/D$, was fixed to be 0.25. Center-to-center distance values between the jets used are 2*D*, 3*D*, 4*D*, and 5*D*. The cross section of the nozzles is taken to be square.

Fig. 2 displays the projection of flow lines on the mid vertical x–z plane for $R_m = 0$, 0.5, and 1.0 at $Re = 200$ and $X_n = 4$. The flow lines on an x–z plane are obtained from the U and W components of the velocity vectors on that plane. For the case of fixed heated plate, $R_m = 0$, the first column of jets, counted from the symmetry plane on the left, form wall jets upon impingement on the bottom plate which spreads out radially in the absence of any crossflow effect. After the first column, crossflow emanating from the upstream jets interferes and deflects the downstream jets. The jet deflection increases at downstream side of the array. The forward flowing wall jets, formed by the second column of jets, interact with the crossflow and form ground horseshoe vortices close to the impingement plate, which wraps around the impinging jet like a scarf. After the third column, the jet is bent more under the influence of increasing crossflow such that no wall jet can form in the reverse direction of the crossflow. As a result a ground vortex cannot form in front of the jets and the crossflow is squeezed on the plate by the jet. For such small jet-to-plate distance used, the crossflow effect is higher and, as a result, the crossflow forms a blanket over the bottom plate, preventing jet impingement. For $R_m > 0$, the horseshoe formed near the first column and with the same way as in the case of no moving plate. The movement of the plate plays as a crossflow effect to the first column jets. The velocity ratio of the moving plate increases the crossflow as a result a ground vortex cannot form in front of the second and third column jets (Fig. 2 b and c). After the first column, the blanket start form above the bottom plate. The thickness of the blanket increases in a downstream direction due to the increasing of the crossflow resulting from the upstream jets and the accelerating of the surface movement, as a result increases in jet deflection. For the range of the velocity ratio of the moving plate used, the flow stricture is not affected by increasing R_m. Projection of flow lines around first four column of jets, on different horizontal planes are shown in Fig. 3 for $Re = 200$, $R_m = 1.0$, and $X_n = 4$. For high elevations, $Z = 0.225$ and 0.125, the jet spreads out radially at the symmetry plane of the domain. At a distance closer to the bottom plate, $Z = 0.025$, the ground horseshoe vortices formed around the first

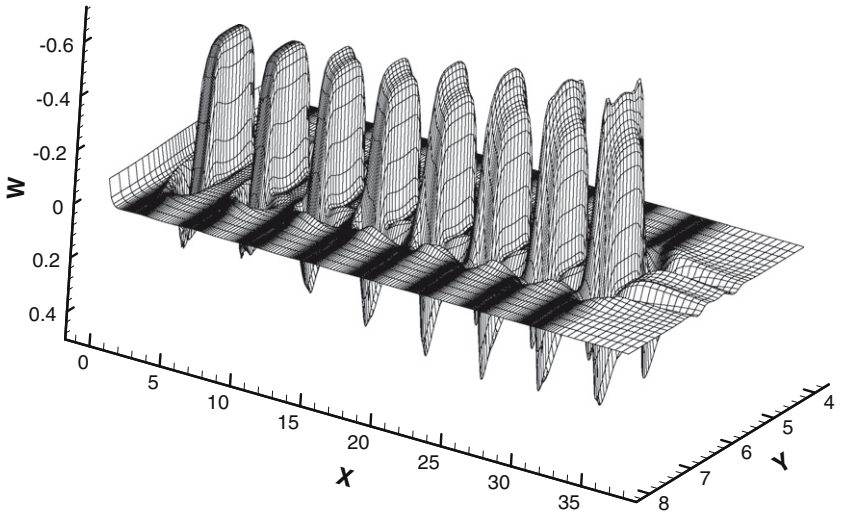

Fig. 4. The three-dimensional plots of the W velocity for $Re = 200$, $R_m = 1.0$, and $X_n = 4$ at the horizontal cross section $Z = 0.075$.

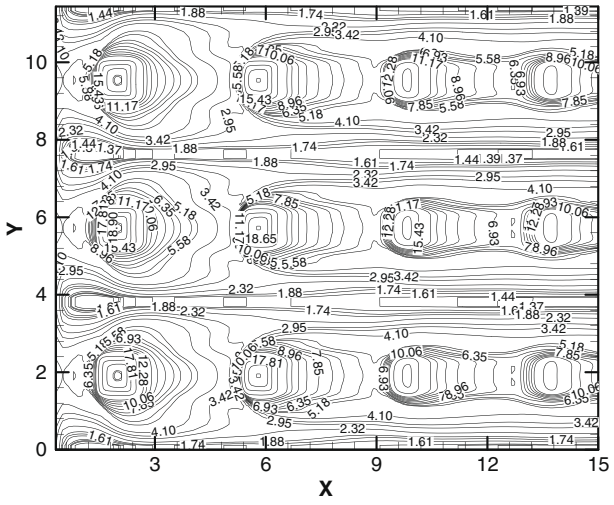

Fig. 5. Contour plot of the Nusselt number for $Re = 200$, $R_m = 1.0$, and $X_n = 4$.

column. After the first column of jets no reverse flow can form at the collision points of jets for this rather low nozzle-to-plate spacing where the strong crossflow bends the jets in the flow direction. A carpet plot of the W component of the velocity is shown in Fig. 4 at the horizontal plane $Z = 0.075$ for the conditions given in Fig 3. The maximum jet velocity occurs at the jet axis for the first column of jets. For the next columns, the downward bending of the crossflow by the impinging jets augments the vertical velocity and, as a result, the peak of the vertical velocity shifts from the jet axis toward the upstream side of the crossflow. Two additional off-center peaks also form which are offset by about $0.5D$ from the jet axes along y-direction for jets in the third and eighth columns. The formation of the off-center velocity peaks along y-direction is similar to that encountered in single and multiple laminar jets with no crossflow [32–34].

The distribution of the vertical velocity component directly influences the heat transfer characteristics as shown in Fig. 5, which displays the Nusselt number distribution for the velocity profile shown in Fig. 4. Heat transfer is expressed in terms of the local Nusselt number as

$$Nu = \frac{hD}{k} \tag{6}$$

where h is the local convection heat transfer coefficient defined as

$$h = \frac{q''_w}{t_w - t_j} \tag{7}$$

The local Nusselt number is also equal to the non-dimensional heat flux and calculated from $Nu(x,y) = \partial T/\partial Z|_{wall}$.

In Fig. 5 the jet stagnation areas are distinguishable clearly as locally high Nusselt number regions with lower heat transfer between jet stagnation zones. At extreme upstream locations in the channel the Nusselt number distribution is about concentric with highest Nusselt number in the center. Downstream, the local heat transfer becomes a superposition of the stagnation flow and the accumulated channel flow, which elongates the Nusselt number distribution in the crossflow direction. The streamwise profiles of the local Nusselt number along the central line joining the jet centers is depicted in Fig. 6 corresponding to the velocity profiles shown in Fig. 2. The oscillatory behavior of the Nu profiles illustrates the regions of high and low transport directly beneath and between the jets, respectively. Such strong oscillations in the local Nusselt number have been observed previously in jet arrays with crossflow (Metzger et al. [3], Florschuetz et al. [4], and Garrett and Webb [6]). The amplitude of the periodic oscillations is attenuated where the peaks diminish and the valleys increase in magnitude as one proceeds in the downstream direction. A general characteristic common is the increasing shift of the peak value of Nu in the downstream direction, which is associated with the increasing crossflow magnitude. In addition, the oscillatory behavior of the Nu profiles is not affected by whether the heated plate is fixed or moving or even by increasing the velocity ratio of the moving plate. The only difference is the heat transfer increase little bit at the left side of the first column jets due to the formation of the horseshoe for the case of $R_m > 0$. Similar result was observed by Yang and Hao [10] with turbulent slot jets with moving surface for the range of velocity ratio of the moving surface between 0.05 and 0.25.

The effect of the jet-to-jet spacing, X_n, on Nusselt number distribution is shown in Fig. 7 for $R_m = 0.5$. The corresponding flow profiles are illustrated through projection of flow lines on the mid vertical plane in Fig. 8. For this small jet-to-plate spacing used, the increasing crossflow downstream forms a layer blanketing the heated plate through which the jets cannot penetrate. As a result the periodic variations in the Nusselt number profile are attenuated downstream the flow. The maximum magnitude of the local Nu is shown under the first column for $X_n = 2$ and then a high reduction under the second column. Where as for $X_n = 3$ the peak of the local Nu for the first and second column is same in magnitude and then high reduction occurs at the third column and shifts downstream at higher X_n values. A close examination of the flow profile shows that at locations of high reduction in the local Nu occurs, at a place a crossflow fluid layer blanketing the bottom plate is start form.

Fig. 9 illustrates the effect of Reynolds number on the profiles of the local Nusselt number distribution along a streamwise line joining jet centers for $X_n = 5$ and $R_m = 1$. For $Re > 200$ secondary peaks are formed downstream the jet axes for first and second column jets as a result of squeezing the crossflow on the plate by the downstream jet. The magnitude of the secondary peak increases by increasing Reynolds number and reduced for the same Re till it vanish as one proceeds downstream direction due to increasing crossflow effect. The increases of the crossflow are enough to start form the crossflow fluid layer blanketing the bottom plate under-

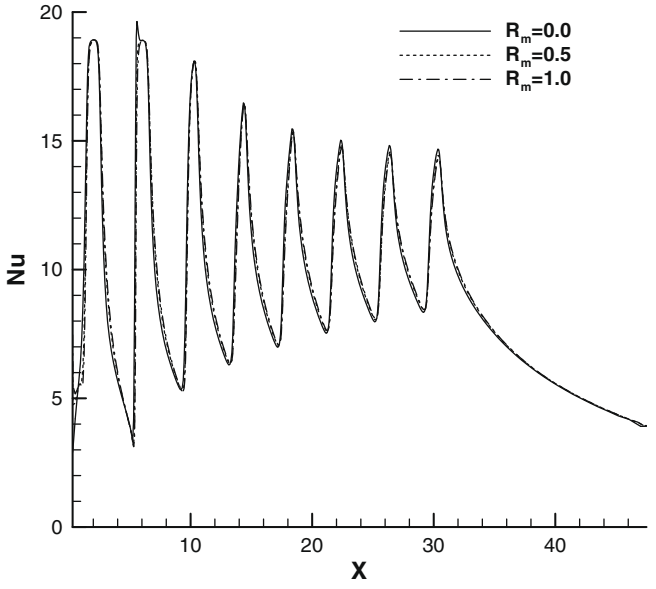

Fig. 6. Effect of velocity ratio R_m on Nusselt number variation for $Re = 200$ and $X_n = 4$.

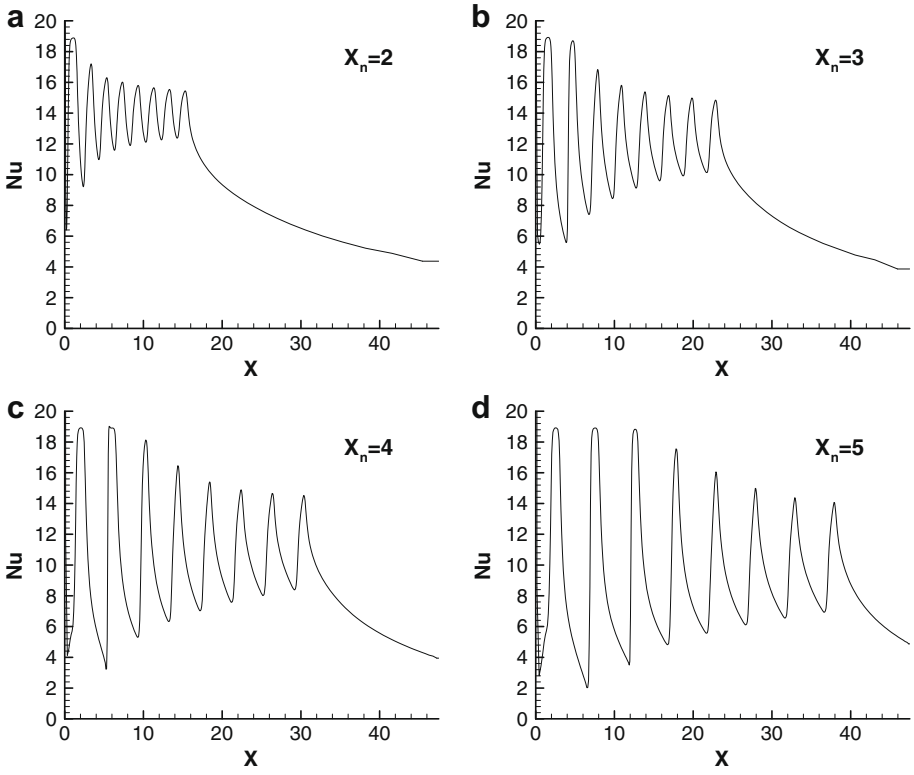

Fig. 7. Effect of jet-to-jet spacing on Nusselt number variation for $Re = 200$ and $R_m = 0.5$.

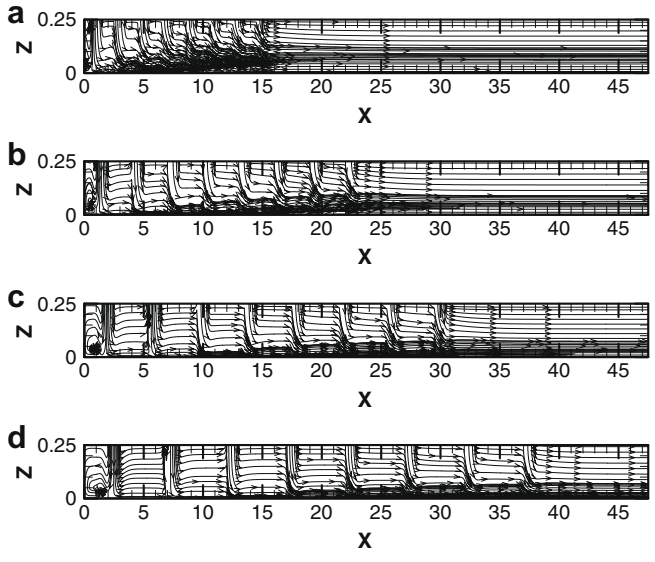

Fig. 8. Projection of flow lines on mid x–z plane for $Re = 200$, $R_m = 0.5$, and for jet-to-jet spacings (a) $X_n = 2$, (b) $X_n = 3$, (c) $X_n = 4$, and (d) $X_n = 5$.

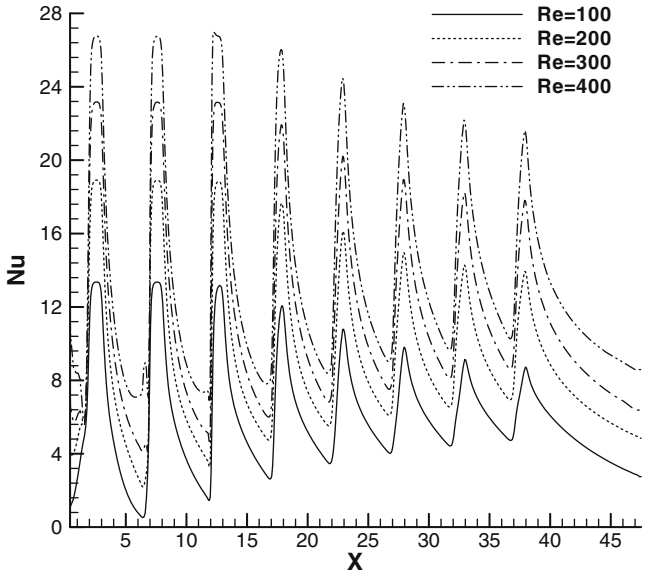

Fig. 9. Effect of Reynolds number on local Nusselt number for $R_m = 1$ and $X_n = 5$.

neath the fourth column jets. Moreover, the increases of the local *Nu* at the left of the first column jets is due to the formation of the horseshoe vortices as result of interact the forward wall jets with the crossflow.

The average Nusselt number values for various surface speed ratio and different jet-to-jet spacing are given in Table 1. The averaging is done over the total impingement surface area cooled by the 24 jets, which is equal to 24 X_n^2. For the same surface velocity ratio, R_m, the average Nusselt decreases at larger jet-to-jet spacings. This is expected because the jet array with a small jet-to-jet

Table 1
Average Nusselt number for various jet configurations.

	Nu	
R_m	0.25	1.0
$X_n = 2$	10.437	10.58
$X_n = 3$	7.28	7.4
$X_n = 4$	5.14	5.34
$X_n = 5$	3.797	4.19

spacing has the smallest surface area cooled per jet, which is equal to X_n^2. Equivalently, the mass flow rate per unit surface area is highest for an array system with smaller X_n. This means that the surface area cooled by one jet in an array having $X_n = 4$ is cooled by two jets in an array with $X_n = 2$. The average Nusselt number increases with surface velocity ratio, R_m.

5. Conclusions

A three-dimensional numerical study has been undertaken to determine the flow and heat transfer characteristics of impinging laminar array of square jets on a moving surface. The results indicate a rather complex flow field with horseshoe vortices formed around the first column of jets due to the crossflow created by the moving surface. The velocity ratio of the moving plate increases the crossflow as a result a ground vortex cannot form in front of the second and third column jets compared with the case of fix surface. For the range of the velocity ratio of the moving plate used, the flow structure in general is not affected by increasing R_m.

The streamwise profile of the Nusselt number exhibit strong periodic oscillations, spatially. The amplitude of the periodic oscillations is attenuated as one proceeds in the downstream direction. In addition, the oscillatory behavior of the *Nu* profiles is not affected by whether the heated plate is fixed or moving or even by increasing the velocity ratio of the moving plate.

For $Re > 200$ secondary peaks are formed downstream the jet axes for first and second column jets as a result of squeezing the crossflow on the plate by the downstream jet. The magnitude of the secondary peak increases by increasing Reynolds number and reduced for the same *Re* till it vanish as one proceeds downstream direction due to increasing crossflow effect.

For the same surface velocity ratio, R_m, the average Nusselt decreases at larger jet-to-jet spacings. The average Nusselt number increases with surface velocity ratio, R_m.

References

[1] R. Gardon, J.C. Akfirat, Heat transfer characteristics of impinging two-dimensional air jets, ASME J. Heat Transfer 88 (1966) 101–108.
[2] D.M. Kercher, W. Tabakoff, Heat transfer by a square array of round air jets impinging perpendicular to a flat surface including the effect of spent air, J. Eng. Power 92 (1970) 73–82.
[3] D.E. Metzger, L.W. Florschuetz, D.I. Takeuchi, R.D. Behee, R.A. Berry, Heat transfer characteristics for inline and staggered arrays of circular jets with crossflow of spent air, J. Heat Transfer 101 (1979) 526–531.
[4] L.W. Florschuetz, R.A. Berry, D.E. Metzger, Periodic streamwise variations of heat transfer coefficients for inline and staggered arrays of circular jets with crossflow of spent air, ASME J. Heat Transfer 102 (1980) 132–137.
[5] N.T. Obot, T.A. Trabold, Impingement heat transfer within arrays of circular jets: Part 1. Effects of minimum intermediate, and complete crossflow for small and large spacings, ASME J. Heat Transfer 109 (1987) 872–879.
[6] K. Garrett, B.W. Webb, The effect of drainage configuration on heat transfer under an impinging liquid jet array, ASME J. Heat Transfer 121 (1999) 803–810.
[7] K. SubbaRaju, E.U. Schlunder, Heat transfer between an impinging jet and a continuously moving surface, J. Heat Mass Transfer 10 (1977) 131–136.
[8] A.R.H. Van Heiningen, A.S. Mujumdar, W.J.M. Douglas, Flow and heat transfer characteristics of a turbulent slot jet impinging on a moving wall, in: Abstracts of the Symposium on Turbulent Shear Flows, Pennsylvania State University, University Park, PA 1, 1977, pp. 3.9–3.15.
[9] J. Senter, C. Solliec, Flow field analysis of a turbulent slot air jet impinging on a moving flat surface, Int. J. Heat Fluid Flow 28 (2007) 708–719.
[10] Y.T. Yang, T.P. Hao, Numerical studies of three turbulent slot jets with and without moving surface, Acta Mech. 136 (1999) 17–27.
[11] J. Chen, T. Wang, D.A. Zumbrunnen, Numerical analysis of convective heat transfer from a moving plate cooled by an array of submerged planar jets, Numer. Heat Transfer A 26 (1994) 141–160.
[12] D.A. Zumbrunnen, Convective heat and mass-transfer in the stagnation region of a laminar planar jet impinging on a moving surface, J. Heat Transfer 113 (1991) 563–570.
[13] D.A. Zumbrunnen, F.P. Incorpera, R.A. Viskanta, Laminar boundary layer model of heat transfer due to a nonuniform planer jet impinging on a moving plate, J. Heat Mass Transfer 27 (1992) 311–319.
[14] H. Chattopadhyay, G. Biswas, N.K. Mitra, Heat transfer from a moving surface due to impinging slot jets, J. Heat Transfer 124 (2002) 433–440.
[15] H. Chattopadhyay, S.K. Saha, Simulation of laminar slot jets impinging on a moving surface, J. Heat Transfer 124 (2002) 1049–1055.
[16] H. Chattopadhyay, Effect of surface motion on transport processes due to circular impinging jets – a numerical study, J. Dry. Technol. 24 (2006) 1347–1351.
[17] H. Chattopadhyay, S.K. Saha, Numerical investigations of heat transfer over a moving surface due to impinging knife-jets, Numer. Heat Transfer A 39 (2001) 531–549.
[18] Wu-Shung Fu, Ke-Nan Wang, Wen-Wang Ke, An investigation of a block moving back and forth on a heat plate under a slot jet, Int. J. Heat Mass Transfer 44 (2001) 2621–2631.
[19] H. Chattopadhyay, S.K. Saha, Turbulent flow and heat transfer from a slot jet impinging on a moving plate, Int. J. Heat Fluid Flow 24 (2003) 685–697.
[20] Wu-Shung Fu, Ching-Chi Tseng, Chien-Ping Huang, Ke-Nan Wang, An experiment investigation of a block moving back and forth on a heat plate under a slot jet, Int. J. Heat Mass Transfer 50 (2007) 3224–3233.
[21] M.A.R. Sharif, A. Banerjee, Numerical analysis of heat transfer due to confined slot-jet impinging on a moving plate, Appl. Therm. Eng. 29 (2009) 532–540.
[22] P. Leonard, A stable and accurate convective modelling procedure based on quadratic upstream interpolation, Comput. Meth. Appl. Mech. Eng. 19 (1979) 59–98.
[23] B.P. Leonard, S. Mokhtari, Beyond first order upwinding: the ULTRA-SHARP alternative for nonoscillatory steady-state simulation of convection, Int. J. Numer. Meth. Eng. 30 (1990) 729–766.
[24] B.P. Leonard, J.E. Drummond, Why you should not use 'hybrid', 'power law' or related exponential schemes for convective modelling. There are much better alternatives, Int. J. Numer. Meth. Fluids 20 (1995) 421–442.
[25] J.P. Van Doormaal, G.D. Raithby, Enhancements of the SIMPLE method for predicting incompressible fluid flows, Numer. Heat Transfer 7 (1984) 147–163.
[26] H.L. Stone, Iterative solution of implicit approximations of multi-dimensional partial differential equations, SIAM J. Numer. Anal. 5 (1968) 530–558.
[27] W. Hackbush, Iterative Solution of Large Sparse Systems of Equations, Springer, 1994.
[28] H.A.V. van der Vorst, BI-CGSTAB: a fast and smoothly converging variant of Bi-CG for the solution of non-symmetric linear systems, SIAM J. Sci. Stat. Comput. 10 (1989) 1174–1185.
[29] Y. Saad, Iterative Methods for Sparse Linear Systems, PSW Publ. Co., Boston, 1996.
[30] E.M. Sparrow, T.C. Wong, Impingement transfer coefficients due to initially laminar slot jets, Int. J. Heat Mass Transfer 18 (1975) 597–605.
[31] L.B.Y. Aldabbagh, I. Sezai, Three-dimensional numerical simulation of an array of impinging laminar square jets with spent fluid removal, Int. J. Therm. Sci. 43 (2004) 241–247.
[32] I. Sezai, A.A. Mohamad, 3-D simulation of laminar rectangular impinging jets, flow structure and heat transfer, ASME J. Heat Transfer 121 (1999) 50–56.
[33] A. Chatterjee, L.J. Deviprasath, Heat transfer in confined laminar axisymmetric impinging jets at small nozzle-plate distances: the role of upstream vorticity diffusion, Numer. Heat Transfer A 39 (2001) 777–800.
[34] L.B.Y. Aldabbagh, I. Sezai, Numerical simulation of three-dimensional multiple impinging square jets, Int. J. Heat Fluid Flow 23 (4) (2002) 509–518.